SCHOOL OF MECHANICAL, INDUSTRIAL & AERONAUTICAL ENGINEERING

MECN4029A

Mechatronics II assignment 2024 Project B:

Solar Tracker

Student Numbers:

2114240

1827215

679233

1834893

WITWATERSRAND, JOHANNESBURG | INDUSTRIAL & AERONAUTICAL ENGINEERING

Disclosure – Use of Artificial-Intelligence (AI) Generated Content

2024 V2

Students must acknowledge all use of AI.

1. Disclosure: No AI use

☒ I acknowledge that no AI tools/technologies (Grammarly, ChatGPT, Bard, Quillbot, OpenAI etc) were used in the completion of this assessment.

☒ ***I declare that the disclosure is complete and truthful.***

Student number: 2114240
1827215
679233
1834893

Course code: MECN4020A
Date:19/05/2024

EXECUTIVE SUMMARY

South Africa's persistent energy crisis, largely driven by the instability of its aging coal-fired power plants, necessitates alternative energy solutions. Solar energy has emerged as a popular option, but stationary solar panels fail to maximize energy capture. This report proposes a single-axis solar tracking system to enhance the efficiency of solar panels by following the sun's movement, potentially increasing energy production by up to 30%.

This project, focusing on the University of Witwatersrand's South-West Engineering building, explores the development and implementation of a single-axis solar tracker. The approach integrates mechatronics, control systems, and computational tools, specifically leveraging Matlab and Simulink for simulation and control design. The tracker’s performance is analysed during the winter and summer solstices, key periods for assessing energy capture efficiency.

Initial system analysis using Simulink indicated significant initial error and delayed convergence in the uncontrolled solar tracker, undermining its energy efficiency. Stability assessments via Bode and Nyquist plots confirmed the general stability of the uncontrolled system but highlighted performance precision issues.

To resolve these issues, a PID controller was designed and implemented. This controlled system demonstrated marked improvements in tracking accuracy and responsiveness. Stability was affirmed through Nyquist plots, showing no critical encirclement, and root locus analysis, indicating stability at low gains but potential instability at higher gains.

In summary, the PID-controlled solar tracking system significantly enhances solar panel efficiency and reliability, offering a viable and sustainable solution to South Africa’s energy challenges. This innovative approach provides a substantial improvement over stationary solar panels and presents a compelling strategy for institutions like the University of Witwatersrand to achieve energy independence and stability.

TABLE OF CONTENTS

LIST OF FIGURES

LIST OF TABLES

1. INTRODUCTION

South Africa has been under re-construction with the country's need to find alternative power solutions as it is constantly experiencing power cuts nationwide. At the root of South Africa's energy crisis are the country's coal-fired power plants, which are responsible for generating about 95% of the country's electricity [1]. It has been identified that these facilities are old, over-used, and constantly breaking down and have been poorly maintained [1]. Furthermore, the energy crisis has led more South Africans to investigate alternative energy solutions. Most companies and residents are going off grid and are investing in solar energy. Whilst solar energy is a solution it is not highly effective because most solar panels are stationary thus, they don't collect the maximum available energy. This then opens an opportunity for a new solution in the form of a solar tracker system which tracks the sun's movement.

When solar trackers are coupled with solar panels, the panels can follow the path of the sun and produce more renewable energy for use [2]. Through tracking the sun movement more energy can be harnessed, and the efficiency of the solar panels may also increase. There are three solar tracking system available, there is a manual solar tracker which requires an individual to manually turn the panels towards the direction of the sun, then there is a passive tracker which contains liquid with low boiling point that will evaporate when exposed to solar radiation thus tilting the panel and lastly there is an active solar tracker which is more effective as it relies on a motor and hydraulic cylinders to change position and thus track the sun [2].

The active solar tracker can be categorised even further based on which direction they navigate to, there is a single axis tracker which only moves from one axis (east to west) and can increase energy production by 25-30 % more than stationary panels [2]. The dual axis tracker moves within two-axis and can move east-west and north-south and it has the capacity to increase energy production up to 40%. Focusing on the efficiency of the trackers a dual axis tracker can deliver more (10-15) % more energy than the single axis tracker. For the purposes of this analysis single axis movement will be analysed.

These tracking units can be mounted on the roof or ground depending on the size and number of panels being used. Normally panels are kept on the roof and mounted in one direction and angle. Tracking systems offer greater levels of energy output compared to fixed solar arrays because they can follow the sun's movements [3]. Figure 1 shows two single axis tracking schematics for solar tracking.

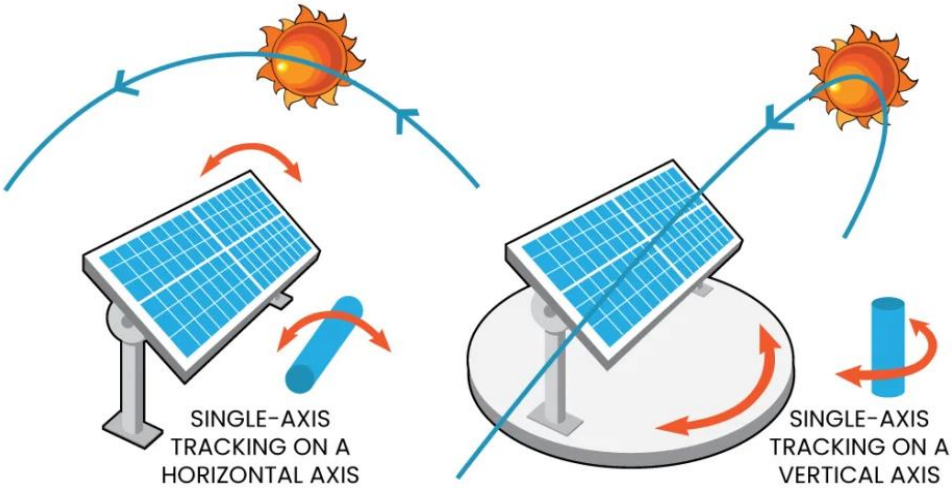

Figure 1:Two single axis tracking units [4]

A scenario where such a solar tracking system will be used will be on a university campus such as The University of Witwatersrand. Due to the ongoing power outages in South Africa, It would be beneficial for solar panels to be installed in such a location as it will allow for the area to function independent of the power grid and result in a continuous power source (assuming they are connected to batteries to store the electricity). The specific location chosen will be the South-West Engineering building as this is where the authors of this document have most of their lectures. The data for the sun motion for the specific location is obtained by SunEarthTools.com and can be seen in the figure below.

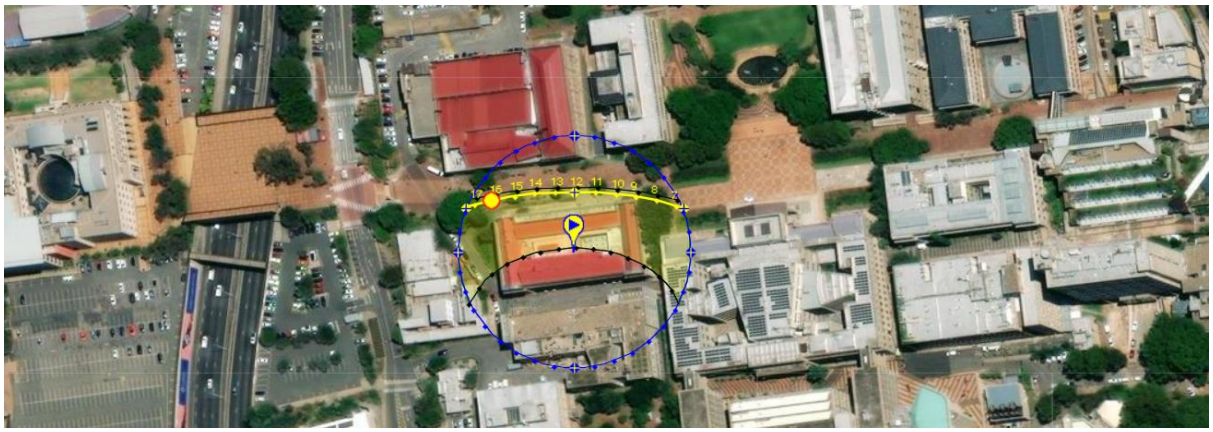

Figure 2: South-West Engineering building at Wits location as seen from above [12].

Analysis for this location will be taken from this position and be analysed for day of tracking. It should be noted that the analysis will be done during the coldest and hottest days of the year namely: the winter solstice and summer solstice respectively.

2. DEVELOPMENT OF SOLAR TRACKING SYSTEM

The development of the tracking system requires a look into mechatronic systems whereby there is a combination of systems, devices and objects combined to work together to accomplish the tracking task. All Earth Solar is one of the few companies that produce solar tracking devices, and their devices incorporate the use of Motors, gears, hydraulic cylinders [3]. These would be the basic start materials, but more will be put in to achieve product requirements and further perform smooth and better. The design process of the solar tracker will require the integration of difference disciplines, figure 3 below is a schematic of our approach to the design process. The tracking system will require electrical systems combine with mechanical systems for the actuating parts. These then require a control system that will make the entire actuator process to behave in the required manner and all this will require a computer in the form of software language that need to be written in order for the control system to control the system behaviour.

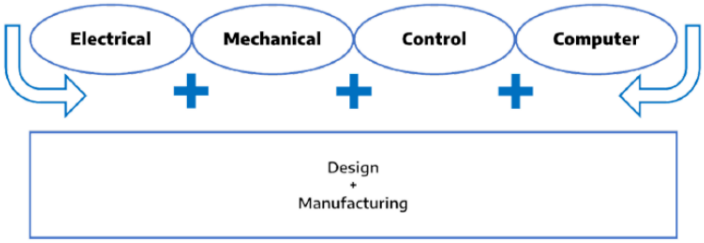

Figure 3: Mechatronics Design Process [11]

Our computing part of the design process directs us to Matlab and Simulink which gives insight on implementing a solar tracker. The introductory work on Matlab and Simulink shows how to simulate and test a controller for a solar panel and tracks the movement of the sun throughout the day [7]. The introductory work shows the integration of electro-mechanical parts that are actuated by a controller to achieve the required work. Furthermore, the sun's movement or information in the form of sun data is required for tracking the sun in a specific geographical area (Wits South-west Engineering building). This will be obtained from a data collecting software called SunEarthTools.com which as mentioned previously will provide the relevant data for both the winter and summer solstice. Using this data the horizontal angle with respect to north that defines the sun's direction along the local horizon can be obtained. This is otherwise known as the azimuth angle.

Using the Matlab and Simulink, the sun data will be passed through the control systems and manipulation of the inputs will take place to obtain the desired outputs. It is important to note that inputs are not only the ones that are inputted through the system, but disturbances and noise are things that our control system will need to handle as part of controlling the plant. Thus, a closed loop or feedback control is required to mitigate noise and disturbance for the control system. Figure 4 is a schematic of a closed loop control that will be required for the control system. An open loop system was not considered as it fails to deal with disturbances and fails to adjust the system to the required point. For solar tracking, a continuous adjustment is required whilst also rejecting disturbances and noise.

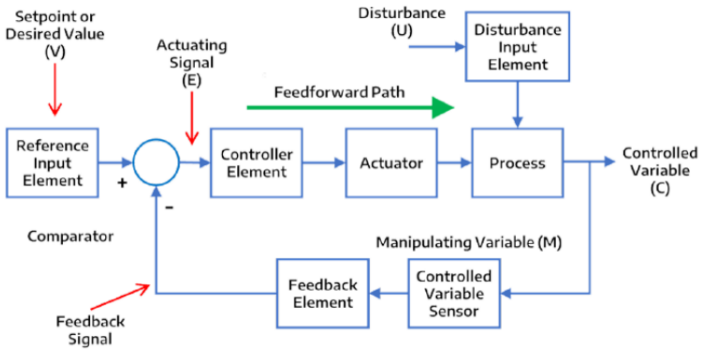

Figure 4: Closed Loop Control System [11]

Figure 4 is a schematic of an Azimuth solar tracker, the work done in Matlab and Simulink uses an azimuth angle to follow the suns movement as depicted the in the figure 5 below. To limit the inclusion of whether sunlight monitoring sensors are needed, it was assumed that the tracker is operating under ideal conditions where it sunny and no clouds are covering or blocking the sun rays.

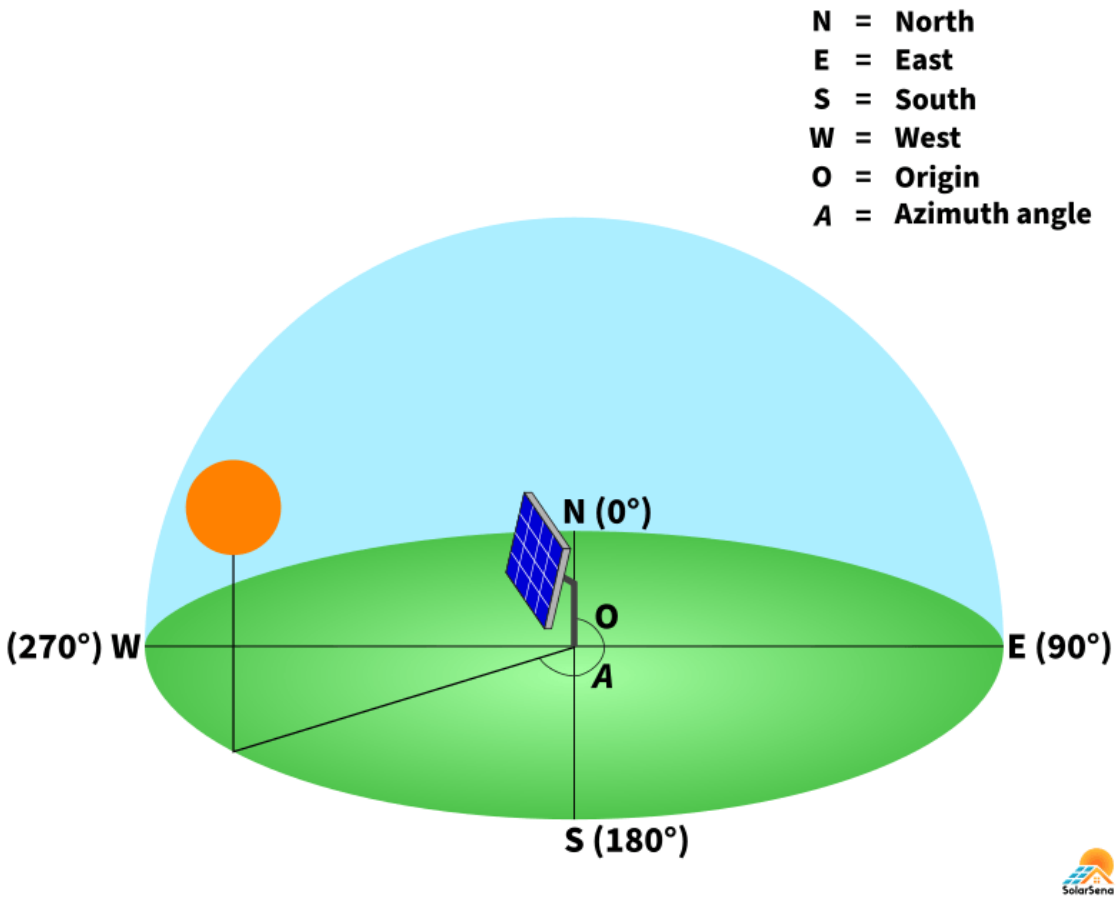

Figure 5: Solar Azimuth Angle [9]

As part of the reference inputs the inclusion of the azimuth angle to the control of tracker suggests that the panel must always point normal to the sun at the required azimuth angle to harness the sun's energy. An optimal angle 'Beta' that points normal to the sun for maximum absorption was found to be $\beta = \pi/4$ [7]. At this angle more energy is harnessed from the sun thus the tracker needs to keep at this angle as it follows the sun. Figure 6 below is a schematic of a model solution tilted to angle beta for harnessing sun rays.

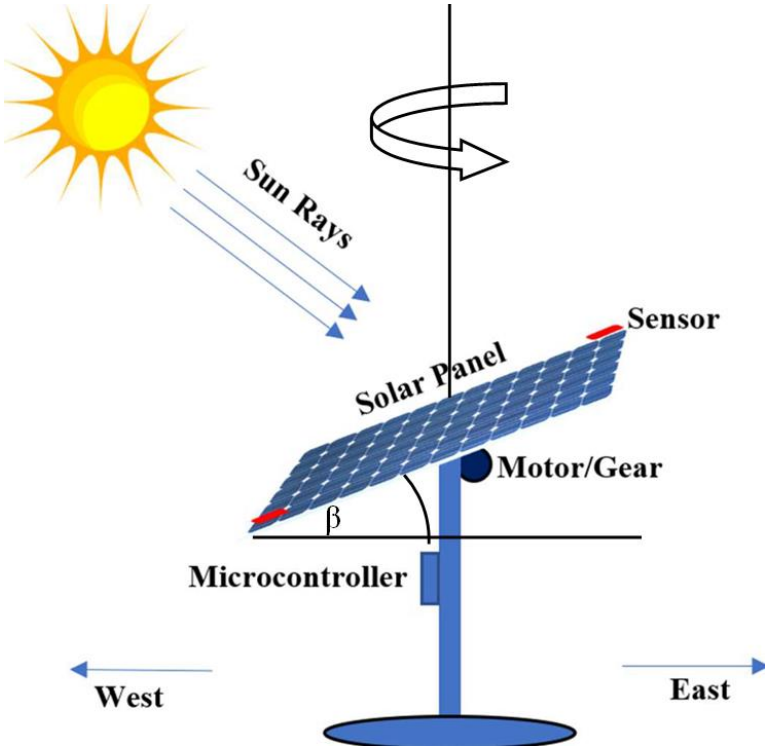

Figure 6: Panel Beta Angle to the Sun

2.1 Modelling

For modelling of the solar tracking system an investigation is required on the performance and behaviour of parts that can be used to build the system. A dynamic system investigation is required of a physical model to understand the required results. The physical model can be further broken down as a mathematical model which then gives an idea of the expected results. Figure 7 shows the process of a dynamic system investigation.

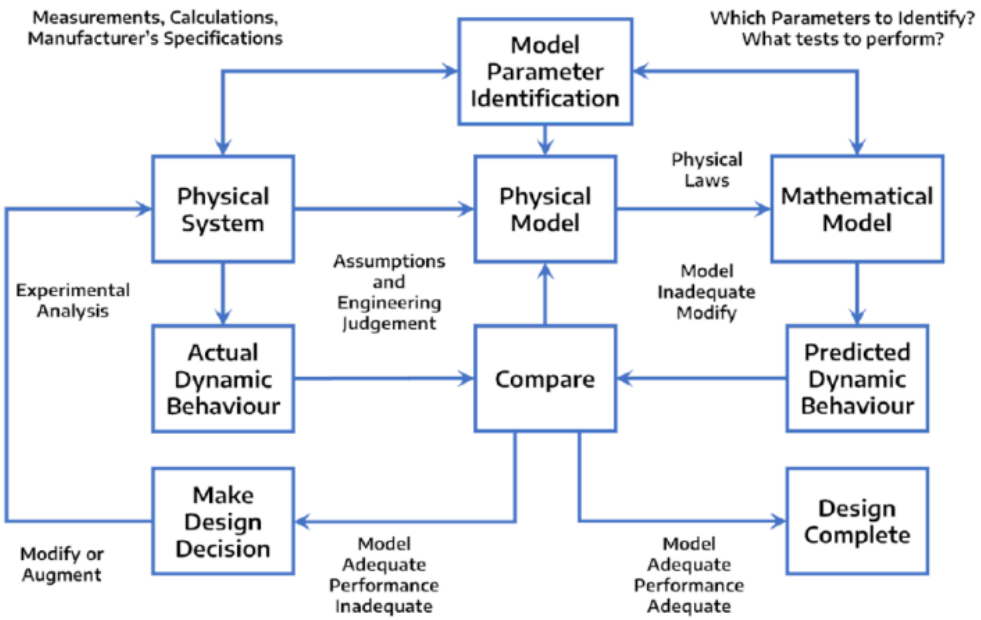

Figure 7:Dynamic System Investigation [11]

2.1.1 Physical Model

Figure 8 shows a picture of a possible working prototype that may be used for tracking. The prototype consists of a single motor which has a shaft and gear connections to allow it to produce smooth rotation and translation. The tracker is required to move at an exceptionally low speed to move with the sun thus it is required that the tracking mechanism be slow and smooth enough to stay in motion with the sun. This system will only be operational during the day from sunrise to sundown and then it will reposition itself to a starting position for the next day.

Figure 8: Solar Tracker Prototype [5]

2.1.2 Expected Performance Specifications

2.1.2.1 Solar Panel Properties

Table 1: Panel Properties [8]

Weight	24kg
Dimensions	2112x1052x35 mm
Brand	Ja Solar
Watts	460 W
Cell Type	Monocrystalline
Product Type	Solar Panel
Efficiency	20.7%
Moment of Inertia J	J
Damping Coefficient K_d	5 Ns/m (Overdamped) [7]

$$J = \frac{m}{12}(l^2 cos^2\beta + d^2 sin^2\beta + w^2) \quad (1)$$

Equation 1: Panel Moment of inertia [10]

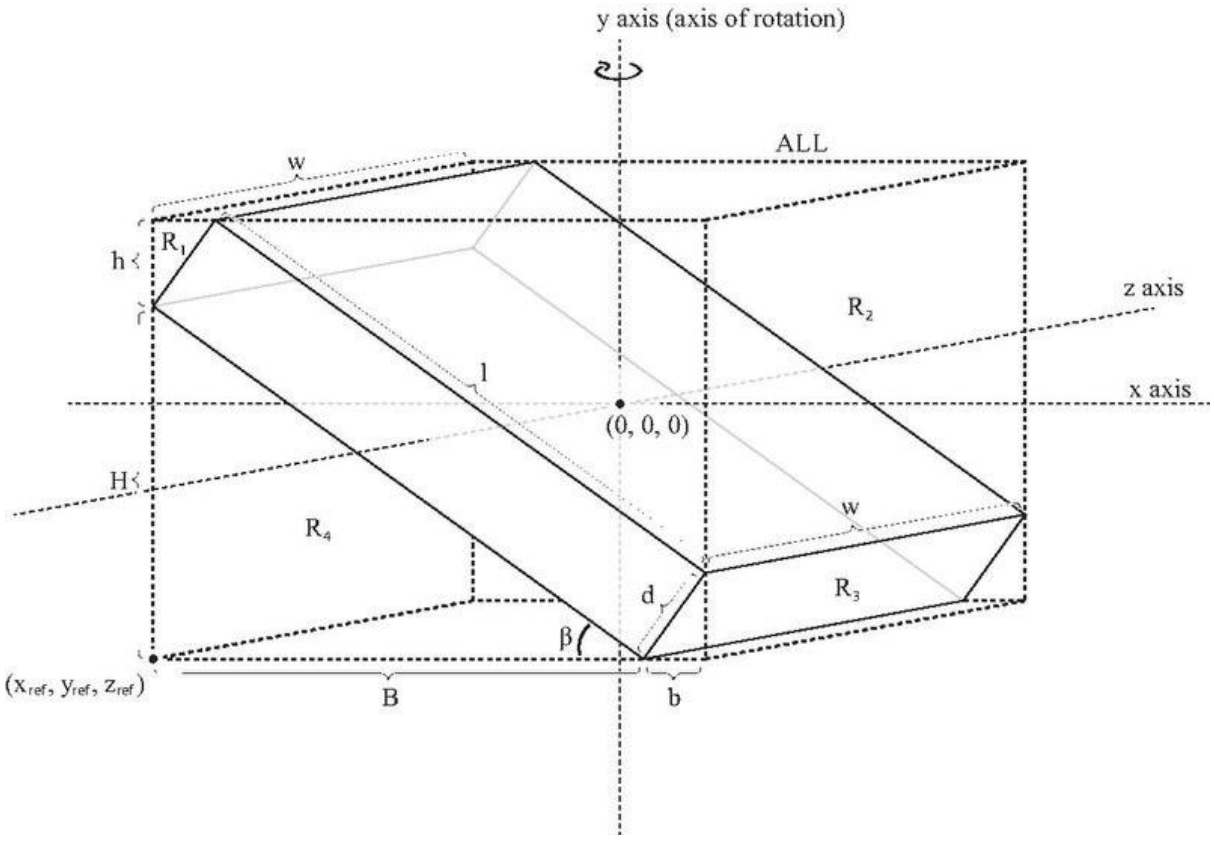

Figure 9: Panel Diagram [10]

2.1.2.2 Motor Properties

In order to drive the system a motor is required to move the system. The motor is a combination electrical and mechanical component which work together to achieve a task. In this case a rotational motion. This motor is supplied with a constant armature current which is proportional to the developed torque. Figure 10 below is a schematic of the Armature Controlled DC motor.

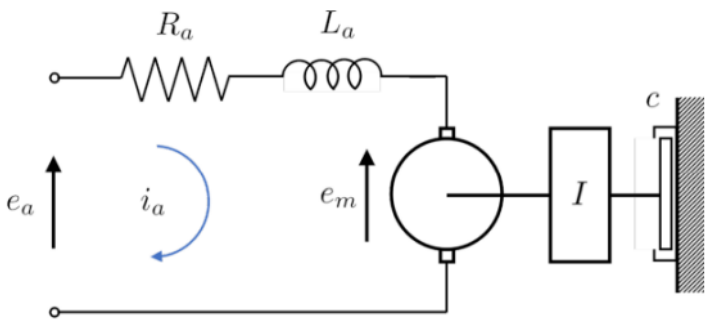

Figure 10: Armature Controlled DC Motor [11]

2.1.3 Mathematical Model

Using the above motor and panel models a mathematical model was derived and the below equations depict the mathematical behaviour of the models in the time domain. Furthermore, through the application of transfer functions the models can further be analysed in a frequency domain. These mathematical models will be used in Matlab and Simulink in order to get a graphical picture of the results.

2.1.3.1 Panel Rotation Angle

This parameter is the translational movement form the motor as the more rotates the position of the angle shall also change with time.

$$\frac{d^2\theta}{dt^2} = \frac{1}{J}\left(T - K_d\frac{d\theta}{dt}\right) \quad (2)$$

2.1.3.2 Motor movement

$$\frac{di}{dt} = \frac{1}{L}\left(T - K_d K_f\frac{d\theta}{dt} - Ri\right) \quad (3)$$

Torque equation:

$$T = K_g K t i \quad (4)$$

2.1.3.3 Model Transfer Functions

$$\Omega = \frac{K_t I_a}{s(Js+K_d)} \quad (5)$$

$$I = \frac{V(s)- K_e\Omega}{Ls+R} \quad (6)$$

2.1.4 Linearization

It is important to note that real systems are nonlinear thus to get an idea of the system results linearization is required. This means that the movement of our system at a certain point will be frozen thus the position, speed and time may be required to be kept static. This process may be done by choosing a suitable equilibrium point then the dynamic response is zero at that point. Using the Taylor Series expansion the system was linearized.

Linearisation

$$\frac{d^2\theta}{dt^2} = \frac{1}{J}\left(T - K_d\frac{d\theta}{dt}\right)$$

$$T = K_g K_t i$$

$$\frac{d^2\theta}{dt^2} + \frac{K_d}{J}\frac{d\theta}{dt} = \left(\frac{K_g K_t i}{J}\right)$$

$$\mathcal{L}\left(\frac{d^2\theta}{dt^2} + \frac{K_d}{J}\frac{d\theta}{dt}\right) = \mathcal{L}\left(\frac{K_g K_t i}{J}\right)$$

$$\frac{di}{dt} = \frac{1}{L}\left(V - K_g k_f\frac{d\theta}{dt} - Ri\right)$$

$$i = \frac{1}{R}\left(V - K_g K_f\frac{d\theta}{dt} - L\frac{di}{dt}\right)$$

$$s^2\theta(s) + \frac{K_d}{J}s\theta(s) = \frac{K_g K_t}{J}\mathcal{L}(i)$$

$$\theta(s)\left(s^2 + \frac{K_d}{J}s\right) = \frac{K_g K_t}{J}\left(\frac{V}{s} - K_g K_f s\theta(s) - \mathcal{L}(i)sL\right)$$

$$\frac{di}{dt} + Ri = \frac{1}{L}\left(V - K_g K_f\frac{d\theta}{dt}\right)$$

$$L\frac{di}{dt} - Ri = V - K_g K_f\frac{d\theta}{dt}$$

$$i = i_0 + \delta i$$

but

$$\frac{d(i+\delta i)}{dt} = \frac{\delta i}{dt}$$

1

$$L\frac{d\delta i}{dt} + R(i_0 + \delta i) = V - K_g K_f \frac{d\theta}{dt}$$

at equilibtium

$$Ri_0 = V$$

$$L\frac{d\delta i}{dt} + R\delta i = -K_g K_f \frac{d\theta}{dt}$$

$$\mathcal{L}\left(L\frac{d\delta i}{dt} + R\delta i\right) = \mathcal{L}\left(-K_g K_f \frac{d\theta}{dt}\right)$$

$$\delta i(s)(Ls + R) = -K_g K_f s\theta_i(s)$$

$$\mathcal{L}(\delta i) = \delta i(s) = \frac{-K_g K_f s\theta_i(s)}{(Ls + R)}$$

$$\theta(s)\left(s^2 + \frac{K_d}{J}s\right) = \frac{K_g K_t}{J}\left(\frac{V}{s} - K_g K_f s\theta(s) - \frac{-K_g K_f s\theta_i(s)}{(Ls + R)}sL - \frac{i_0 R}{s}\right)$$

$$\theta(s)\left(s^2 + \frac{K_d}{J}s\right) = \theta_i(s)\frac{K_g K_t}{J}\left(-K_g K_f s\theta(s) - \frac{-K_g K_f s}{(Ls + R)}sL\right)$$

$$\frac{\theta(s)}{\theta_i(s)} = \frac{s\frac{K_g K_t}{J}\left(-K_g K_f \theta(s) - \frac{-K_g K_f}{(Ls+R)}sL\right)}{\left(s^2 + \frac{K_d}{J}s\right)}$$

3. SYSTEM ANALYSIS OF UNCONTROLLED SYSTEM

3.1 Non-Linear Time Response

To model the response of the solar tracker, Simulink enabled us to examine the intricate system using the dynamic equations derived from the free body diagram with specified inputs, resulting in a continuous system output. As a basis for analysis the block diagram obtained from model 4 from the MathWorks website will be used [13][7]. The following inputs were obtained from the block diagrams provided:

Table 2: Motor and Solar panel parameter [8].

Parameter	Value
Mass of the panel, [kg]	m = 50
Width of the panel, [m]	w = 1.04
Length of the panel, [m]	l = 1.4
Depth of the panel, [m]	d = 0.1
Elevation angle, [rad]	beta = pi/4
Damping constant, [N*m/(rad/s)]	Kd = 5
Moment of inertia, [kg*m^2]	J = m/12*(l^2*cos(beta)^2+d^2*sin(beta)^2+w^2)
Back EMF constant, [V/(rad/s)]	Kf = 0.07
Torque constant, [N*m/A]	Kt = 0.07
Inductance, [H]	L = 1e-5
Resistance, [Ohm]	R = 10
Gear ratio	Kg = 2000

The block diagrams in Simulink used to analyse the nonlinear system is illustrated in the following figures:

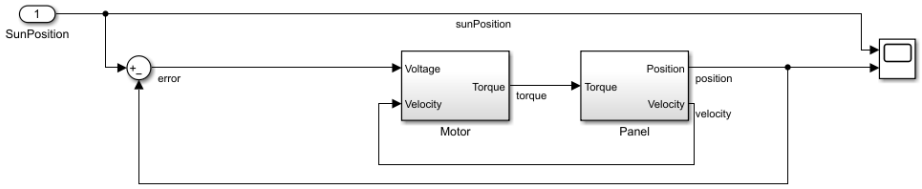

Figure 11: Uncontrolled non-linear block diagram of solar panel and motor.

$$\frac{d^2\theta}{dt^2} = \frac{1}{J}\left(T - K_d\frac{d\theta}{dt}\right)$$

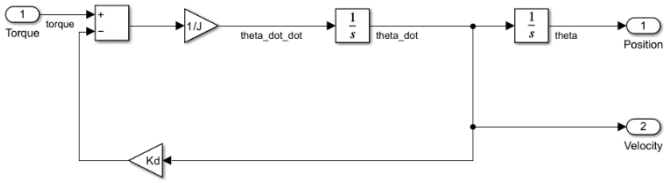

Figure 12: Solar panel block diagram for equation of motion.

$$\frac{di}{dt} = \frac{1}{L}\left(V - K_g K_f\frac{d\theta}{dt} - Ri\right)$$

$$T = K_g K_t\, i$$

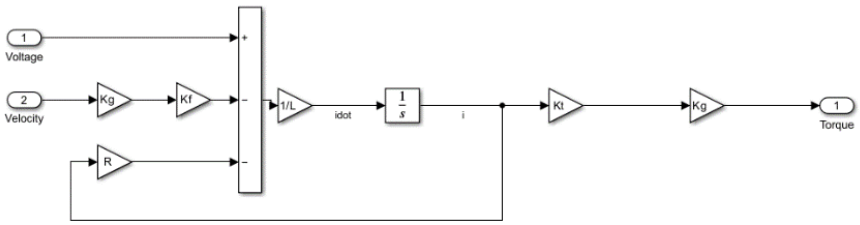

Figure 13: Motor block diagram for motion.

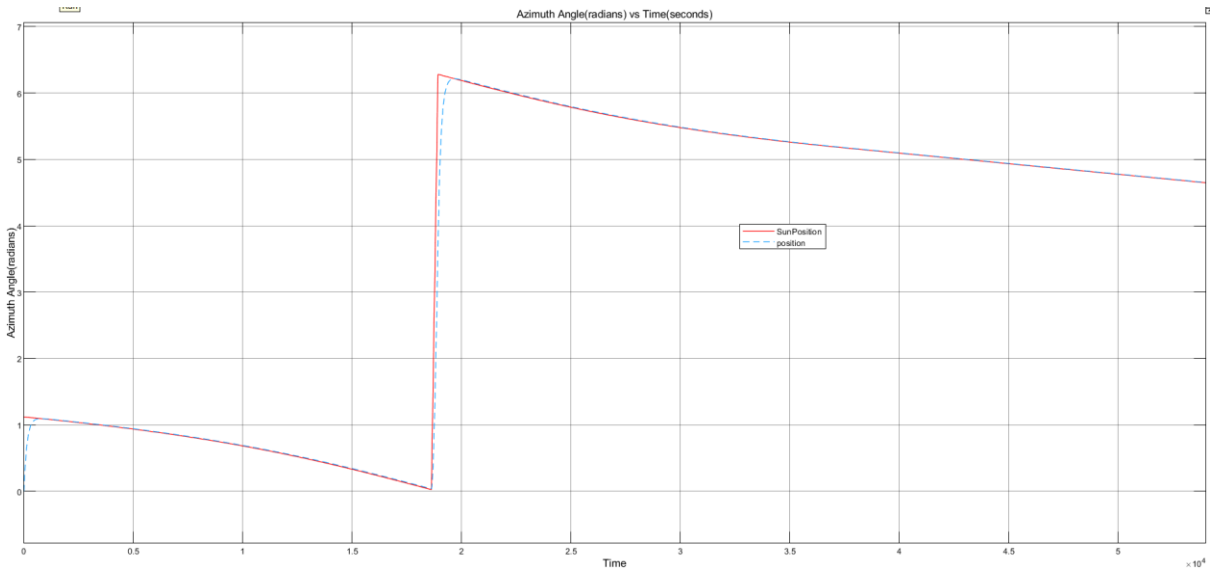

Figure 14: Azimuth angle vs time graph for uncontrolled system.

3.1.1 Evaluation of uncontrolled system

The following observations are made from the responses of the uncontrolled system:

- Initial Discrepancy: There's a noticeable initial error where the system's tracking (dashed line) overshoots the actual sun position (red line).
- Convergence Delay: After the initial overshoot, the system slowly corrects itself but still lags the actual sun position, indicating a delay in response.
- Lack of Precision: Without PID control, the tracking accuracy is compromised, leading to less efficient solar energy capture.
- Improvement Potential: Implementing a PID controller could significantly improve the tracking accuracy by minimizing the initial error and reducing the response time.

3.2 Linear Frequency Response

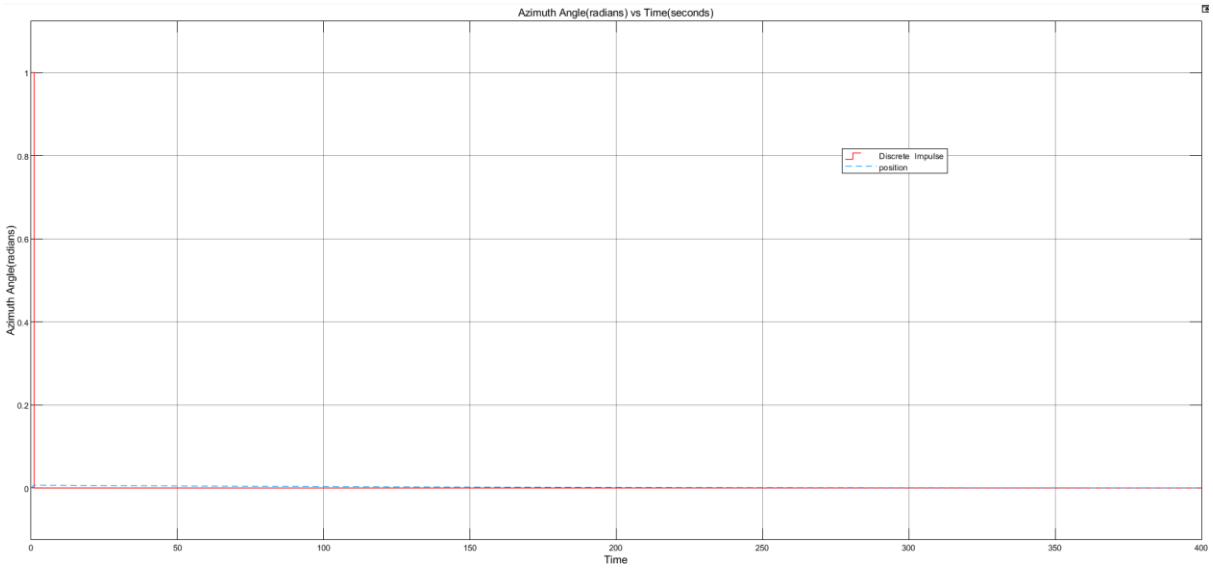

Figure 15: Linear impulse response of uncontrolled system.

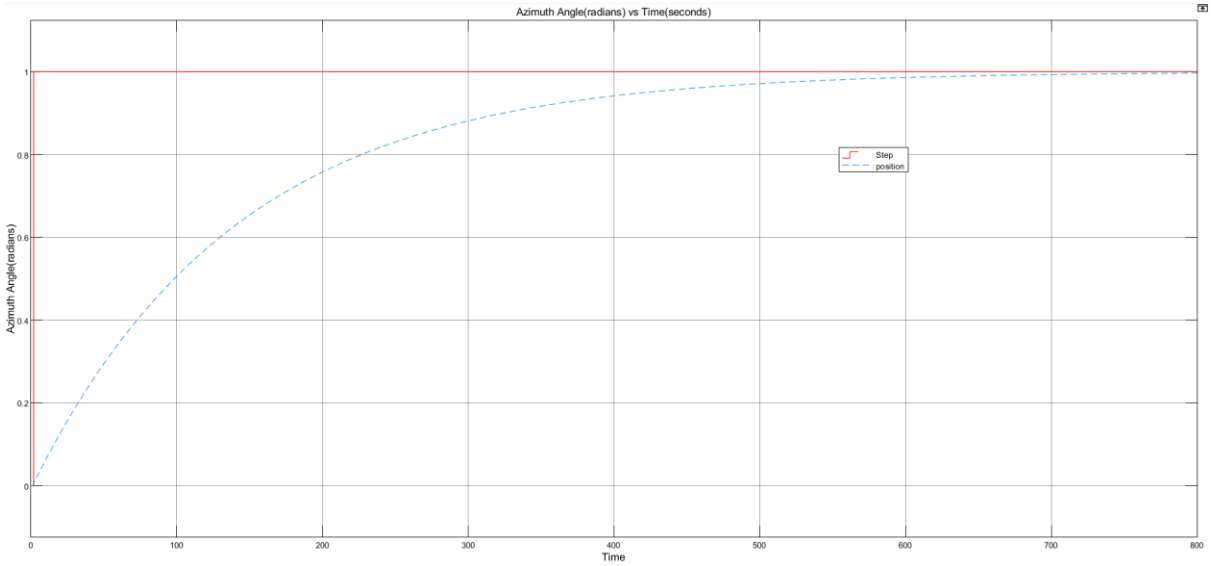

Figure 16: Linear step response of uncontrolled system.

3.2.1 Evaluation of step and impulse response for uncontrolled system

Step Response Behaviour: The graph shows the system's response to a unit-step input (a sudden change from zero to one). The horizontal axis represents time, and the vertical axis represents the system response (output). Initially, the response starts from an initial value (likely zero) and rises exponentially. As time progresses, the response approaches a steady-state value (the dashed line parallel to the time axis).

Key Observations:

- Rise Time: The time it takes for the response to reach a certain percentage (e.g., 90%) of the steady-state value, the system takes 400 seconds or half the time it takes to reach the steady state value to reach a point which is 90 % the steady state value.
- Overshoot: If the response exceeds the steady-state value before settling.
- Settling Time: The time it takes for the response to stay within a specified tolerance band around the steady-state value, for the system it is 800 seconds or around 13 minutes.
- Steady-State Value: The final value that the response approaches, for the step response it is 1.
- Interpretation: A well-tuned control system aims for minimal overshoot, fast rise time, and short settling time. Engineers adjust controller parameters (like PID gains) to optimize these characteristics.
- Conclusion: By analysing the step response, engineers can assess system performance and make necessary adjustments.

4. STABILITY ANALYSIS

4.1 Non-Linear Uncontrolled Plant

By leveraging Matlab to generate Nyquist and Bode plots, we can effectively visualize and analyse the stability characteristics of the system. This approach enables us to make informed decisions about the system's performance and necessary adjustments, ensuring optimal stability and reliability.

4.1.1 Bode Plots

Bode plots provide a detailed view of the system's frequency response, showing both the magnitude and phase across a spectrum of frequencies. These plots are instrumental in identifying the gain and phase margins, which are key indicators of system stability. Gain margin refers to how much gain can be increased before the system becomes unstable, while phase margin indicates how much phase shift can be tolerated before instability occurs. Larger margins generally suggest a more stable and robust system, whereas smaller margins warn of a higher risk of instability.

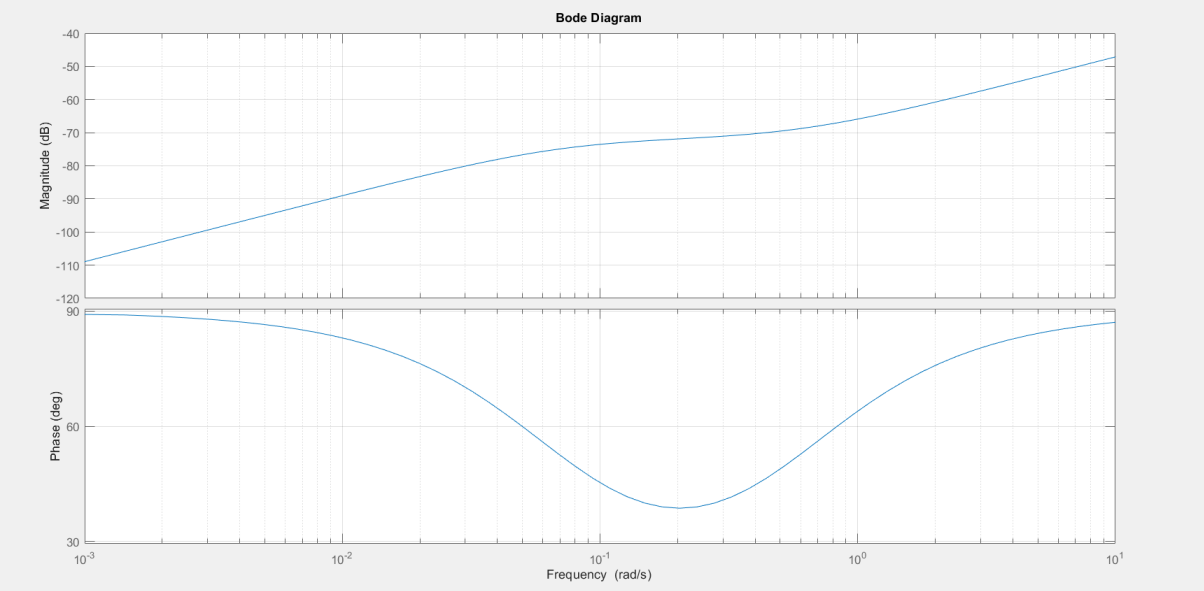

Figure 17: Bode plot for uncontrolled system.

Key observations from this bode plot are:

- Magnitude Plot: The absence of a 0 dB crossover in the magnitude plot suggests that the system does not have a gain of 1 at any frequency within the observed range, which is generally a good sign for stability.
- Phase Plot: The phase plot does not cross -180 degrees, indicating no phase crossover frequency, another indicator that the system may be stable.
- Stability Indicators: Since neither critical crossover point (-180 degrees for phase, 0 dB for gain) is reached, the system is likely to be stable over the observed frequency range.
- Further Analysis Needed: To fully confirm stability, information beyond the displayed frequency range and additional performance criteria, such as phase margin or gain margin, would be necessary.

4.2 Nyquist stability of Linear Plant

The Nyquist criterion is a powerful tool for determining the stability of a closed-loop control system by examining the open-loop frequency response. This method involves plotting the open-loop transfer function in the complex plane to see how it encircles the critical point (-1,0). By analysing this plot, we can predict potential oscillations and determine whether the system will remain stable under given conditions.

4.2.1 Nyquist Plot

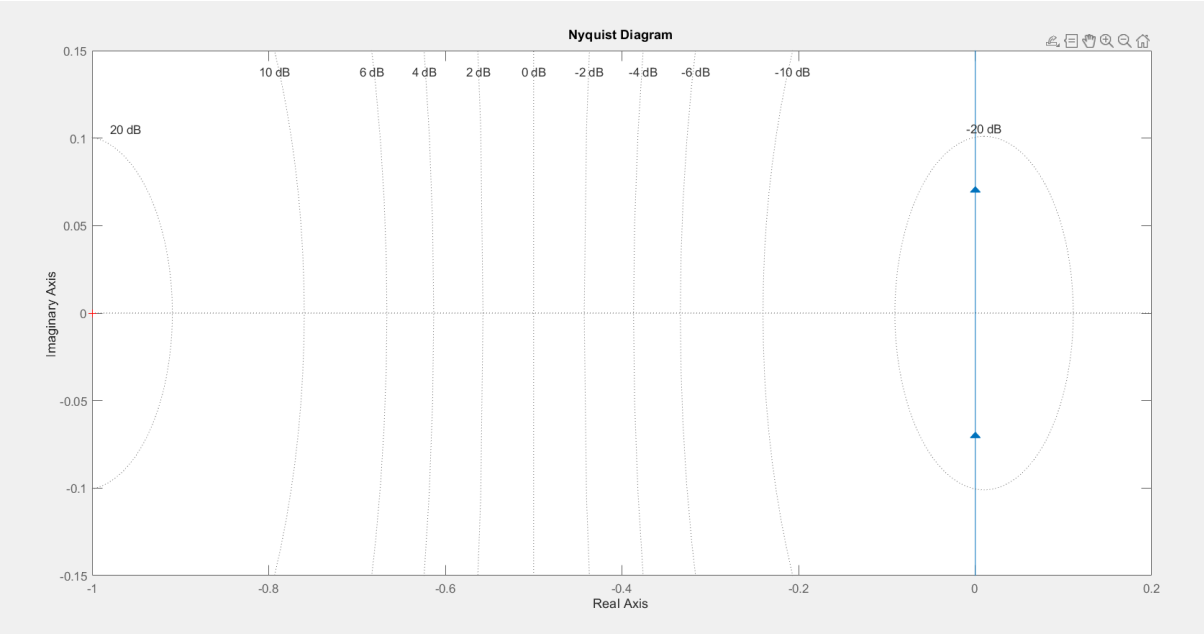

Figure 18: Nyquist plot for uncontrolled system.

Here are the key implications based on the Nyquist plot:

- Stability Analysis: The plot shows how the frequency response of a system changes with frequency. The number of times the plot encircles the origin indicates the number of unstable poles in the system.
- Encirclement: The loop in the plot encircles the origin, which is crucial for stability analysis. If the plot encircles the origin clockwise, it indicates unstable poles.
- Critical Point: The orange dot on the negative real axis likely represents the critical point (-1+0j). The system's stability is determined by the plot's behaviour around this point.
- Implications: The stability of the system can be inferred from the plot. If the plot does not encircle the critical point and has no encirclements of the origin, the system is stable.

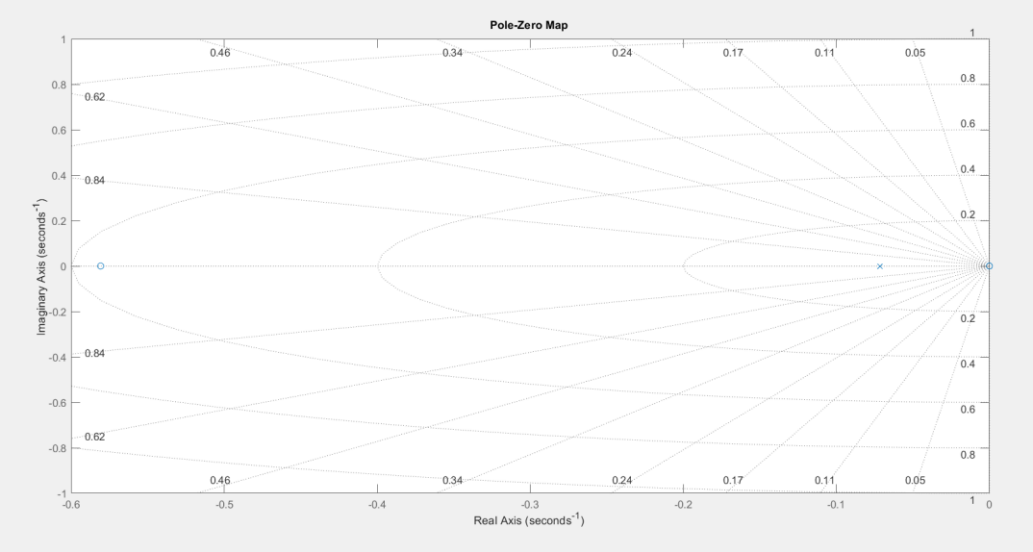

Figure 19: Pole-Zero plot of uncontrolled system.

The key implications of the Pole zero plot are:

- All poles are in the left half of the complex plane (negative real part); therefore, the system is possibly stable.

5. Closed Loop Controller

In control laws the motivation for using feedback in a mechatronics system is to improve linearity, reduce the effects of sensitivity and to also reduce the effects of disturbance inputs [11]. The systems may be affected by a lot of variables some which may not be known in the beginning, and some may arise from noise and disturbances. Feedback control can solve most of these issues since closed loop controllers use measurements of the output to modify the systems actions in order to achieve the intended goals [11].

To assess the control structure of the solar tracker, the system is required to position the solar panel at an azimuth angle theta. This is done by an actuating motor which is applying torque which is translated to a rotary movement. Whilst the panel is rotated at an azimuth angle wind can blow at the direction of the panel and thus induce a disturbance torque to the system.

The governing equation for the control in the time domain and the transfer function in the s domain are written below.

$$\frac{d^2\theta}{dt^2} = \frac{1}{J}\left(T - K_d\frac{d\theta}{dt}\right) \qquad (7)$$

$$\Omega = \frac{K_t I_a}{s(Js+K_d)} = \frac{\Omega}{T} = \frac{1}{s(Js+c)} \qquad (8)$$

K_d represents the damping coefficient thus it can also be written as c. A block diagram is added below to describe the position of the tracker. This is a second order system and will require a suitable control system. It has been noted that combined control modes can give better results and less errors compared to a proportional control or Integral control. The derivative control only works in combination with other controllers. Since Proportion control only reduces the error but cannot eliminate it, an Integral control improves the steady state error but degrades the transient performance. This then suggest two possible control laws a proportional plus integral control or a proportional plus derivative control.

For small c, the gain K_p must be large in order to satisfy the condition of the equation below. Furthermore, if K_p is large then the system becomes under damped.

$$\frac{\theta(s)}{T_d(s)} = \frac{s}{Js^3+cs^2+K_ps+K_I} \qquad (9)$$

$$\frac{\theta(s)}{T(s)} = \frac{K_ps+K_I}{Js^3+cs^2+K_ps+K_I} \qquad (10)$$

$$\zeta = \frac{c}{2\sqrt{JK_p}} \qquad (11)$$

To maintain stability, Routh Hurwits on the S^1 level J, c, K_p and K_i must be none zero and (cK_p - JK_i > 0) in or not to have a sign change. Thus, the PI is not a suitable control.

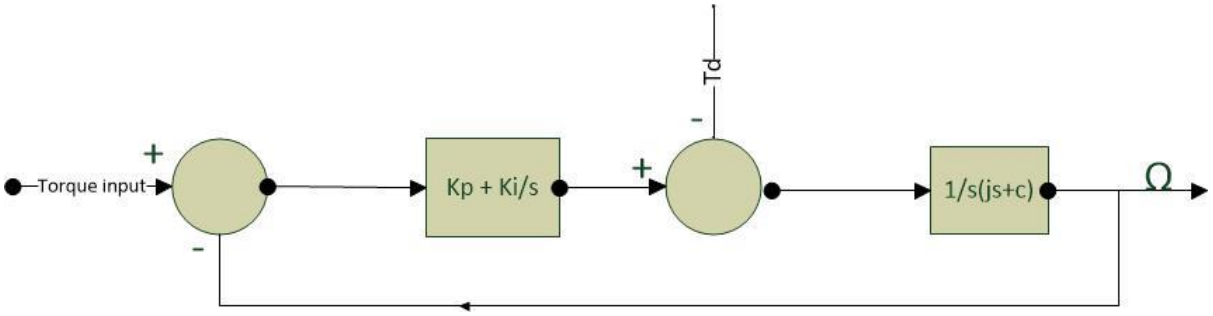

Figure 20 : Proportional Integral block diagram.

Proportional plus derivative control is another possible control for our second order system it can solve our control problem provided the Kp and Kd values are positive. Looking at the damping ratio, Kp is chosen large for reduction in steady state deviation [11]. If there is no damping constant, then the system becomes unstable.

$$\frac{\theta(s)}{T(s)} = \frac{K_p + K_I s}{Js^2 + (c + K_D)s + K_p} \qquad (12)$$

$$\frac{\theta(s)}{T_d(s)} = \frac{1}{Js^2 + (c + K_D)s + K_p} \qquad (13)$$

$$\zeta = \frac{c + K_p}{2\sqrt{JK_p}} \qquad (14$$

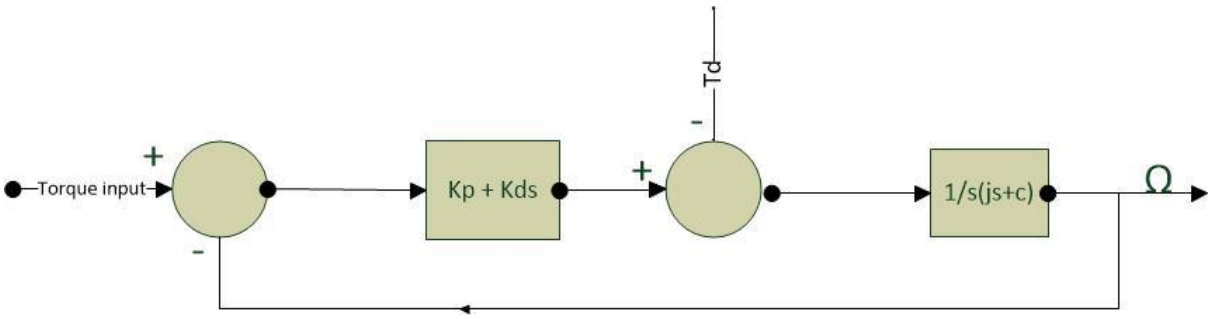

Figure 21: Proportional Derivative Control Block Diagram

This then leaves us to the conclusion that a Proportional Integral Derivative Controller will be best for our system. This controller covers three modes thus it can provide the required results.

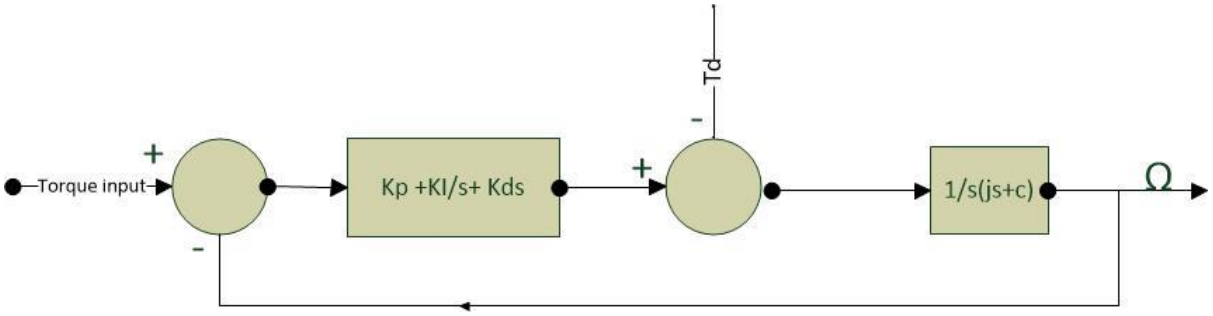

Figure 22 : Proportional Integral Derivative Controller Block Diagram

$$\frac{\theta(s)}{T(s)} = \frac{K_d s^2 + K_p s + K_I s}{Js^3 + (c + K_D)s^2 + K_p s + K_I} \quad (15)$$

$$\frac{\theta(s)}{T_d(s)} = \frac{s}{Js^3 + (c + K_D)s^2 + K_p s + K_I} \quad (16)$$

Routh Hurwitz stability shows that $(c + Kd)Kp - JK_I > 0$)if all these are positive then the system is stable. Further the system has zero steady state error and can be used for step, ramp, impulse or test for errors [11]. This means that a PI and PID are possible solutions, PID will be used as it is more robust.

5.1 Proportional-Integral-Derivative

In the Laplace domain, the PID controller transfer function is given by:

$$G_{PID}(s) = K_p + K_i/s + K_d$$

- *Kp* is the proportional gain.
- *Ki* is the integral gain.
- *Kd* is the derivative gain.

The values chosen where initially that of the MathsWorks model which set the *Kp* value to 240, *Ki* to 180 and *Kd* to 1[7]. Analysis is done for these values and is seen to conform to the motion of the sun's path thus these values remained unchanged.

The diagram below shows the step response of the PID-controlled plant G(s), which has been tuned to meet the specified performance requirements optimally.

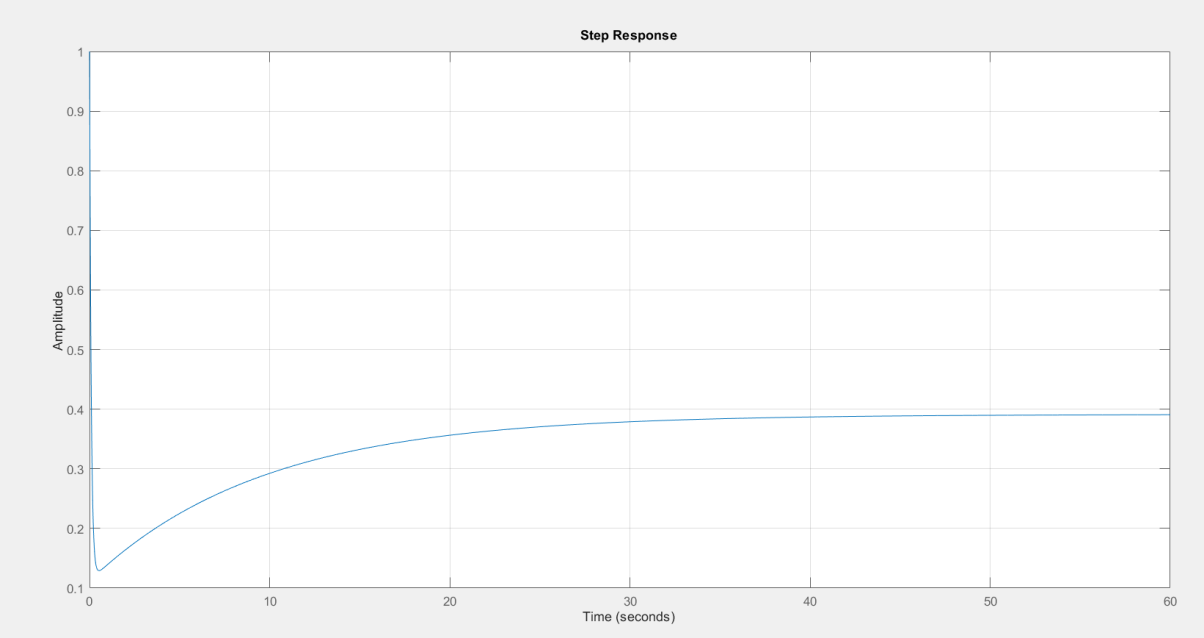

Figure 23: Step response for PID controlled system.

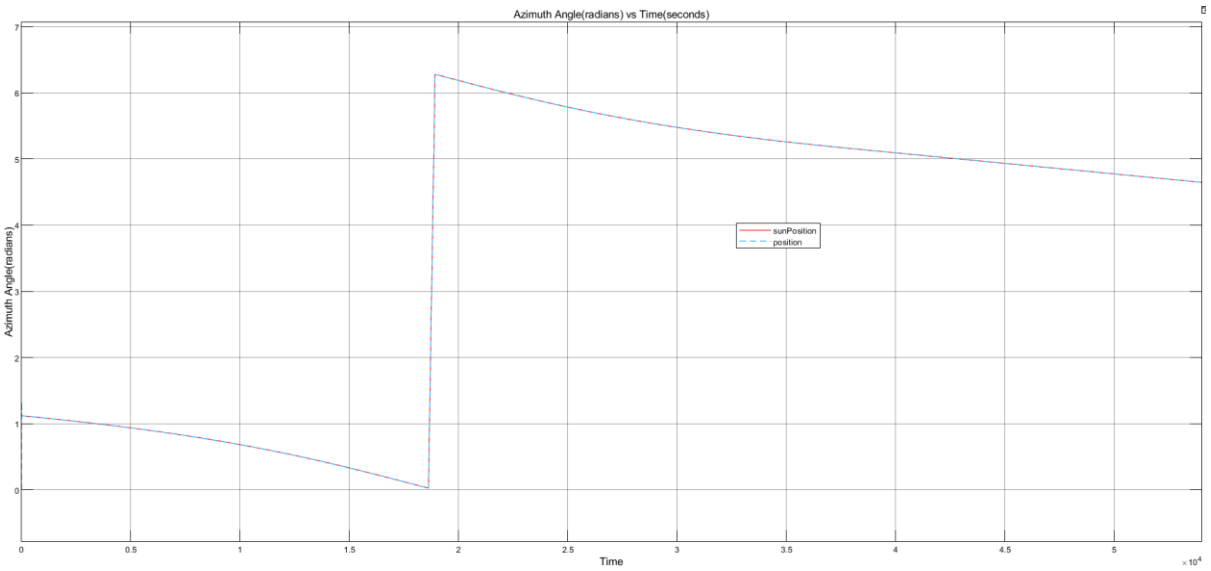

Figure 24: Azimuth angle vs time graph for PID controlled system.

The following block diagram is obtained from Simulink:

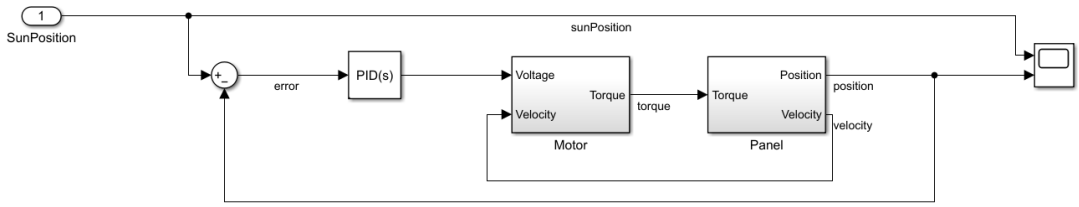

Figure 25: Block diagram od controlled system.

Through implementing the PID control, from the figure above, the controlled system ensures that the solar tracker can follow the suns position more accurately than the uncontrolled system, thus justifying the use of PID.

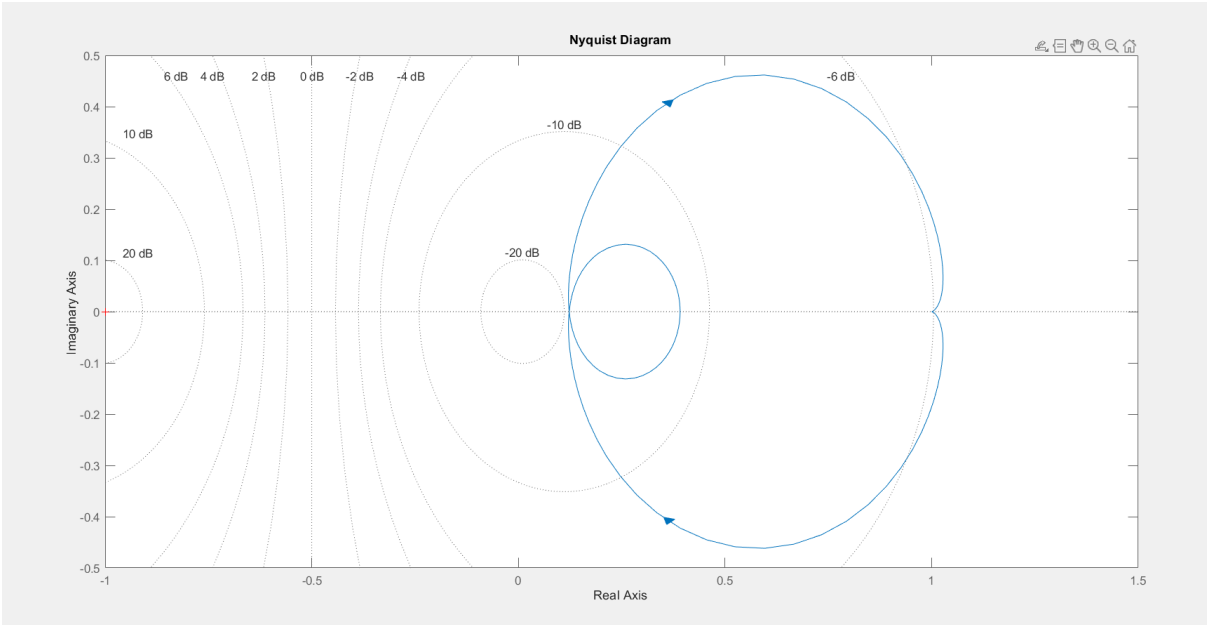

Figure 26: Nyquist diagram for PID controlled system.

5.1.1 Evaluation

The Nyquist plot shows the frequency response of a system. The x-axis represents the real part (Re) of the transfer function, and the y-axis represents the imaginary part (Im). The plot consists of two solid blue curves. The following behaviours are observed:

- Loop Encirclement: The larger blue curve encircles the origin (0,0) in a clockwise direction. The smaller blue curve is inside the larger one and encircles the origin in a clockwise direction.
- Stability Implications: The key point for stability analysis is whether the Nyquist plot encircles the point (-1,0) on the real axis. Since the larger loop does not encircle (-1,0), we can conclude that the system is stable. The absence of right half plane zeros (encirclements around the origin) indicates stability.
- Decibel Contours: The concentric dashed circles represent different decibel levels (dB). These contours help visualize the gain margin of the system.

7.2 Root Locus

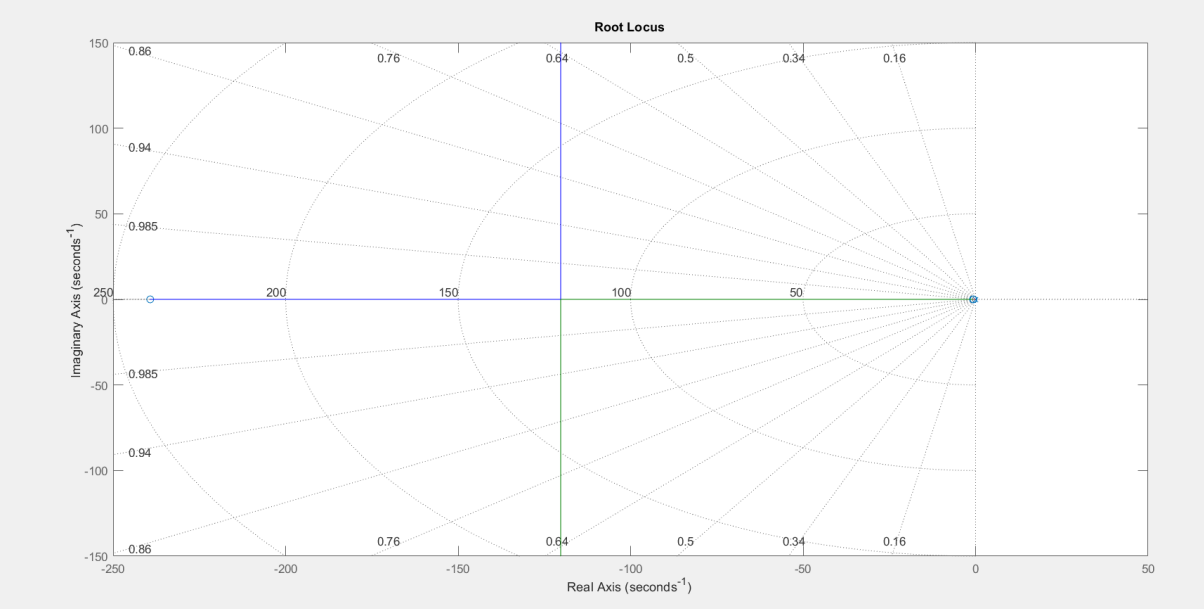

Figure 27: Root locus plot for PID controlled system.

5.2.1 Evaluation

Implications of the Root Locus Plot:

- Pole Movement: The two distinct loci originate from different points on the negative real axis. Both loci converge towards points on the positive real axis. Each locus represents a pair of complex conjugate poles. As the gain increases, the poles move towards the right half of the s-plane.

- Stability Analysis: Stability depends on the location of the poles, if any pole crosses into the right half plane (positive real axis), the system becomes unstable. If all poles remain in the left half plane (negative real axis), the system is stable**.** In this case the poles start from the left half plane (negative real axis). As the gain increases, they move towards the right half plane. If the gain exceeds a certain value, the system will become unstable.

6. CONCLUSION AND EVALUATION OF CONTROLLED SYSTEM

The controlled system, utilizing the PID controller, ensures accurate sun tracking compared to an uncontrolled system, while the Nyquist plot confirms stability, and the root locus analysis provides insights into pole movement. The given root locus plot suggests that the system is stable for low gains. However, as the gain increases, the poles move towards the right half plane, potentially leading to instability. The Nyquist plot suggests that the system is stable. The clockwise encirclement of the origin without crossing the (-1,0) point indicates a stable closed-loop system.

7. REFERENCES

1. *Understanding South Africa's energy crisis - african energy chamber* (2023) *African Energy Chamber - Leading chamber of successful networks, transactions and partnerships*. Available at: https://energychamber.org/understanding-south-africas-energy-crisis/ (Accessed: 23 April 2024).
2. Lane, C. (1969) *What is a solar tracker and is it worth the investment?, Compare solar companies, solar panels, and solar prices*. Available at: https://www.solarreviews.com/blog/are-solar-axis-trackers-worth-the-additional-investment (Accessed: 19 April 2024).
3. *.Allearth Solar Tracker* (2024) *AllEarth Renewables*. Available at: https://www.allearthrenewables.com/solar-products/solar-tracker/ (Accessed: 19 April 2024).
4. (No date a) *Bing*. Available at: https://www.bing.com/images/search?view=detailv2&form=SBIHVR&lightschemeovr=1&iss=SBI&q=imgurl%3Ahttps%3A%2F%2Ffrontend-cdn.solarreviews.com%2Fsingle-axis-solar-tracking.png&pageurl=https%3A%2F%2Fwww.solarreviews.com%2Fblog%2Fare-solar-axis-trackers (Accessed: 19 April 2024).

5. (No date a) *Bing*. Available at: https://www.bing.com/images/search?view=detailV2&ccid=0b2%2BE8n6&id=B54BCD9F44F0C8B5080E3F56A8BA619850B3C148&thid=OIP.0b2-E8n6rz84j6vIHXWI_AHaIZ&mediaurl=https%3A%2F%2Fwww.solarslewdrive.com%2Fphoto%2Fsolarslewdrive%2Feditor%2F20210201153659_68856.png&cdnurl=https%3A%2F%2Fth.bing.com%2Fth%2Fid%2FR.d1bdbe13c9faaf3f388fabc81d7588fc%3Frik%3DSMGzUJhhuqhWPw%26pid%3DImgRaw%26r%3D0&exph=771&expw=680&q=Dual%2BAxis%2BSolar%2BTracker&simid=608030351793659672&form=IRPRST&ck=248696C4FAD83BB1F39EE4D11D7C2AD2&selectedindex=97&itb=0&ajaxhist=0&ajaxserp=0&vt=0&sim=11 (Accessed: 23 April 2024).

6. Glueck, E. (2020) *Introduction to worm gearing - bodine - gearmotor blog, Bodine*. Available at: https://www.bodine-electric.com/blog/introduction-to-worm-gearmotors/ (Accessed: 23 April 2024).
7. *Getting started with simulink* (no date) *MATLAB & Simulink*. Available at: https://www.mathworks.com/videos/getting-started-with-simulink-69027.html (Accessed: 23 April 2024).
8. *Ja Solar 460W monocrystalline solar panel: Silver Frame: MC4 - Solar Advice* (2023) *Solar Advice* -. Available at: https://solar.co.za/product/ja-solar-460w-monocrystalline-solar-panel-silver-frame-mc4 (Accessed: 23 April 2024).
9. Sena, S. (2022) *Solar Azimuth Angle Calculator & Solar Panels, SolarSena*. Available at: https://solarsena.com/solar-azimuth-angle-calculator-solar-panels/ (Accessed: 23 April 2024).
10. *List of moments of inertia* (2024) *Wikipedia*. Available at: https://en.wikipedia.org/wiki/List_of_moments_of_inertia#cite_note-9 (Accessed:23 April 2024).
11. Mechatronics II 2024 Lecture Notes Compiled by Dr A Panday
12. Info@sunearthtools.com (no date) *Sun Position, Calculation of sun's position in the sky for each location on the earth at any time of day*. Available at: https://www.sunearthtools.com/dp/tools/pos_sun.php (Accessed: 10 May 2024).

13. *'Getting started with simulink for controls' example files* (no date) *File Exchange - MATLAB Central*. Available at: https://www.mathworks.com/matlabcentral/fileexchange/73257-getting-started-with-simulink-for-controls-example-files (Accessed: 20 May 2024).

8. APPENDIX

Code:

```
% Solar panel and motor parameters
m = 50; % Mass of the panel, [kg]
w = 1.04; % Width of the panel, [m]
l = 1.4; % Length of the panel, [m]
d = 0.1; % Depth of the panel, [m]
beta = pi/4; % Elevation angle, [rad]
Kd = 5; % Damping constant, [N*m/(rad/s)]
J = m/12*(l^2*cos(beta)^2+d^2*sin(beta)^2+w^2); % Moment of inertia, [kg*m^2]
Kf = 0.07; % Back EMF constant, [V/(rad/s)]
Kt = 0.07; % Torque constant, [N*m/A]
L = 1e-5; % Inductance, [H]
R = 10; % Resistance, [Ohm]
Kg = 2000; % Gear ratio, []
% Transfer function variables
a1 = Kd;
a2 = J;
a3 = Kg*Kt;
a4 = L;
a5 = R;
a6 = Kg^2*Kf*Kt;
% Transfer function G1(s) = Theta(s)/V(s)
% Coefficients for Theta(s)
coeffTheta2 = a2;
coeffTheta1 = a1;
% Coefficients for V(s)
coeffV1 = a4*a5 + a6;
coeffV0 = a3*a5;
% Laplace transforms
s = tf('s');
ThetaCoeff = coeffTheta2*s^2 + coeffTheta1*s;
VCoeff = coeffV1*s + coeffV0;
% Transfer function G1
G1 = ThetaCoeff/VCoeff;
% Bode plot for uncontrolled plant
figure('Name', 'Bode plot for G1(s)')
bode(G1)
grid on
% Nyquist plot for uncontrolled plant G1(s)
figure('Name', 'Nyquist plot for uncontrolled plant G1(s)')
nyquist(G1)
grid on
% Poles and Zeros of G1
figure('Name', 'Poles and Zeros of G1')
pzplot(G1)
grid on
% Note: Modify the following section with your desired PID controller values and
controlled system analysis
%-----------------------------------------------------------------
% CONTROLLED SECTION
```

```
% PID gains
Kp1 = 240;
Ki1 = 180;
Kd1 = 1;
% PID equation
C1 = pid(Kp1, Ki1, Kd1);
% Step function for PID controlled system
H1 = C1*G1;
G1PID = feedback(H1, 1);
t = 0:0.01:60;
figure('Name', 'PID controlled step response for G1')
step(G1PID, t)
grid on
% Nyquist plot for PID controlled plant G1(s)
figure('Name', 'Nyquist plot for PID controlled plant G1(s)')
nyquist(G1PID)
grid on
% Root locus with PID controller
figure('Name', 'Root Locus with PID Controller')
rlocus(C1*G1)
grid on
```

Sun Data: Winter[12]

Elevation	Azimuth	AR	hour				Hours	Minutes	Seconds	Seconds
-0,833	116,77	2,038021	05:12:39				5	12	39	0
0,64	115,96	2,023884	05:20:00				5	20	0	441
1,65	115,42	2,014459	05:25:00				5	25	0	741
2,67	114,89	2,005209	05:30:00				5	30	0	1041
3,69	114,36	1,995959	05:35:00				5	35	0	1341
4,71	113,84	1,986883	05:40:00				5	40	0	1641
5,74	113,33	1,977982	05:45:00				5	45	0	1941
6,77	112,83	1,969255	05:50:00				5	50	0	2241
7,8	112,33	1,960528	05:55:00				5	55	0	2541
8,84	111,84	1,951976	06:00:00				6	0	0	2841
9,89	111,36	1,943599	06:05:00				6	5	0	3141
10,93	110,88	1,935221	06:10:00				6	10	0	3441
11,98	110,41	1,927018	06:15:00				6	15	0	3741
13,03	109,94	1,918815	06:20:00				6	20	0	4041
14,09	109,48	1,910786	06:25:00				6	25	0	4341
15,15	109,03	1,902932	06:30:00				6	30	0	4641
16,21	108,58	1,895079	06:35:00				6	35	0	4941
17,27	108,13	1,887225	06:40:00				6	40	0	5241
18,34	107,69	1,879545	06:45:00				6	45	0	5541
19,41	107,26	1,87204	06:50:00				6	50	0	5841
20,48	106,82	1,864361	06:55:00				6	55	0	6141
21,56	106,4	1,85703	07:00:00				7	0	0	6441
22,63	105,97	1,849525	07:05:00				7	5	0	6741
23,71	105,55	1,842195	07:10:00				7	10	0	7041
24,79	105,13	1,834865	07:15:00				7	15	0	7341
25,88	104,72	1,827709	07:20:00				7	20	0	7641
26,96	104,31	1,820553	07:25:00				7	25	0	7941
28,05	103,9	1,813397	07:30:00				7	30	0	8241
29,14	103,49	1,806241	07:35:00				7	35	0	8541
30,23	103,09	1,79926	07:40:00				7	40	0	8841
31,32	102,68	1,792104	07:45:00				7	45	0	9141
32,42	102,28	1,785123	07:50:00				7	50	0	9441

Sun Data: Summer[12]

Elevation	Azimuth	AR	hour				Hours	Minutes	Seconds	Seconds
-0,833	116,77	2,038021	05:12:39				5	12	39	0
0,64	115,96	2,023884	05:20:00				5	20	0	441
1,65	115,42	2,014459	05:25:00				5	25	0	741
2,67	114,89	2,005209	05:30:00				5	30	0	1041
3,69	114,36	1,995959	05:35:00				5	35	0	1341
4,71	113,84	1,986883	05:40:00				5	40	0	1641
5,74	113,33	1,977982	05:45:00				5	45	0	1941
6,77	112,83	1,969255	05:50:00				5	50	0	2241
7,8	112,33	1,960528	05:55:00				5	55	0	2541
8,84	111,84	1,951976	06:00:00				6	0	0	2841
9,89	111,36	1,943599	06:05:00				6	5	0	3141
10,93	110,88	1,935221	06:10:00				6	10	0	3441
11,98	110,41	1,927018	06:15:00				6	15	0	3741
13,03	109,94	1,918815	06:20:00				6	20	0	4041
14,09	109,48	1,910786	06:25:00				6	25	0	4341
15,15	109,03	1,902932	06:30:00				6	30	0	4641
16,21	108,58	1,895079	06:35:00				6	35	0	4941
17,27	108,13	1,887225	06:40:00				6	40	0	5241
18,34	107,69	1,879545	06:45:00				6	45	0	5541
19,41	107,26	1,87204	06:50:00				6	50	0	5841
20,48	106,82	1,864361	06:55:00				6	55	0	6141
21,56	106,4	1,85703	07:00:00				7	0	0	6441
22,63	105,97	1,849525	07:05:00				7	5	0	6741
23,71	105,55	1,842195	07:10:00				7	10	0	7041
24,79	105,13	1,834865	07:15:00				7	15	0	7341
25,88	104,72	1,827709	07:20:00				7	20	0	7641
26,96	104,31	1,820553	07:25:00				7	25	0	7941
28,05	103,9	1,813397	07:30:00				7	30	0	8241
29,14	103,49	1,806241	07:35:00				7	35	0	8541
30,23	103,09	1,79926	07:40:00				7	40	0	8841
31,32	102,68	1,792104	07:45:00				7	45	0	9141
32,42	102,28	1,785123	07:50:00				7	50	0	9441